Which triatomic monohalosilylenes, monohalogermylenes, and monohalostannylenes (HMX) fluoresce or phosphoresce and why? An ab initio investigation

Which Triatomic Monohalosilylenes, Monohalogermylenes, and Monohalostannylenes (HMX) Fluoresce or Phosphoresce and Why? An Ab Initio Investigation

by

Riccardo Tarroni[1)] and Dennis J. Clouthier[2a)]

[1] *Dipartimento di Chimica Industriale "Toso Montanari", Università di Bologna, Viale Risorgimento 4, 40136 Bologna, Italy*

[2]*Ideal Vacuum Products, LLC, 5910 Midway Park Blvd. NE, Albuquerque, NM 87109*

[a)] Author to whom correspondence should be addressed: djc@idealvac.com

ABSTRACT

The possibilities of emission from the $\tilde{A}\,^1A''$ and $\tilde{a}\,^3A''$ excited states of the triatomic halosilylenes, halogermylenes, and halostannylenes (HMX, M=Si, Ge, Sn, X = F, Cl, Br and I) have been explored in a series of extensive *ab initio* calculations. The triplet states are found to have deep bonding wells supporting an extensive manifold of vibrational levels which could give rise to observable triplet-singlet phosphorescence. The $\tilde{a}$ - $\tilde{X}$ band systems of the halosilylenes are calculated to occur at the red edge of the visible and are likely to be very weak. In contrast, the HGeX and HSnX triplet-singlet spectra are shifted 1000 – 2000 cm^{-1} to the higher energy and are expected to be significantly stronger due to increased spin-orbit coupling, making the spectra viable targets for experimental investigations. The $\tilde{A}$ - $\tilde{X}$ fluorescence is found to be limited by the possibility of HMX ($\tilde{A}\,^1A''$) → H (^{2}S) + MX ($^2\Pi$) dissociation in the excited state leading to the expectation that HGeF is unlikely to be detectable by laser-induced fluorescence (LIF) spectroscopy. The HSiX and HGeX species with known LIF spectra are found to have deeper $\tilde{A}$ state bonding wells and minimal or no calculated barriers to dissociation. It is generally found that the intensity in their LIF spectra tails off due to a diminution of vibrational overlap rather than the abrupt opening of a dissociation channel.

Few of the HSnX species are known experimentally. HSnF and DSnF are found to dissociate very low down in the $\tilde{A}$ state vibrational manifold and are predicted to be unobservable by LIF spectroscopy. The LIF spectrum of HSnCl is expected to consist of only 1 or 2 bands, with slightly more activity for DSnCl, precisely as has recently been found experimentally. HSnBr and DSnBr have deeper $\tilde{A}$ state bonding wells and their LIF spectra are thus likely to be more extensive. Although HSnI/DSnI are calculated to have deep bonding wells with respect to the H + MX dissociation, predictions are complicated by the existence of a global small bond angle minimum and the opening of a second SnH + I dissociation channel.

I. INTRODUCTION

Over the last two decades, the Clouthier group have studied the electronic spectra of the halosilylenes and halogermylenes (HSiX; HGeX, X = F, Cl, Br, I) by laser induced fluorescence (LIF) in supersonic expansions. The $\widetilde{A}$ - $\widetilde{X}$ LIF and emission spectra of HSiF,[1-3] HSiCl,[4,5] HSiBr,[5,6] HSiI,[7,8] HGeCl,[9,10] HGeBr[11] and HGeI[11,12] and their deuterated isotopologues have been recorded and the ground and excited state molecular structures determined. Recently, we have extended these investigations to the corresponding halostannylenes, successfully observing the LIF spectra of HSnCl and DSnCl.[13] In some cases, we have been unable to observe fluorescence under conditions which should have produced the reactive intermediate (HGeF)[9] or the LIF spectra were only detectable by excitation of the lowest few vibronic levels in the excited state, particularly for the stannylenes. In SnH_2 and SnD_2, it seemed clear from fluorescence lifetime and hole burning measurements that upper state dissociation was the cause of the breaking off of the fluorescence.[14] Since these are all small triatomic molecules, it is unlikely that other nonradiative processes would occur with appreciable efficiency. We speculated that *ab initio* theory might be employed to predict the fluorescence properties of any particular species by studying the excited state potential relative to the expected dissociation products. In this work, we report the results of a comprehensive theoretical study and compare the predictions with the available experimental data.

There have been a substantial number of theoretical papers studying various aspects of the properties of the HMX (M=Si, Ge, Sn; X=F, Cl, Br, I) molecules. Here, we very briefly review the most recent contributions relevant to the present work. Mok and coworkers have used *ab initio* theory and Franck-Condon simulations to study the molecular structures and $\widetilde{A}$ - $\widetilde{X}$ absorption and emission spectra of HSiF/DSiF,[15] HSiCl/DSiCl[16] and HGeCl/DGeCl,[17] including vibrational anharmonicity Their predicted geometries, vibrational frequencies and spectra were in generally good accord with experiment. Contemporaneously, Lin *et al* published similar studies of the ground and first excited singlet states of HGeCl/DGeCl,[18] HGeBr/DGeBr[19] and HSiCl/DSiCl.[20] They emphasized the importance of *3d* orbitals in the Ge containing species and found very good agreement between theory and experiment for the molecular geometries, vibrational frequencies and simulations of spectra.

In 2011, Ehara et al.[21] used the analytical energy gradients of the direct symmetry-adapted cluster–configuration interaction method to predict the absorption and emission spectra of the HSiF/DsiF and HsiCl/DsiCl species. Good agreement was found in all cases between theory and experiment, reinforcing once again the viability of using *ab initio* methods to predict the ground and excited singlet state properties of the HMX species. Finally, in two papers, Bundhun *et al.* used density functional theory (DFT) methods to predict the ground and excited triplet state geometries and energies of a variety of HMX species including HGeX[22] and HSnX.[23] The reader is referred to the original references for a more complete background to the various diverse theoretical studies of HMX molecules. We are not aware of any theoretical studies of the HMX molecules that directly address the role of excited state dissociation processes in the spectroscopy.

II. COMPUTATIONAL METHODS

The majority of the calculations were undertaken with the Molpro2010 program[24] with limited contributions from the Orca code.[25] For light atoms the Dunning correlation consistent basis sets aug-cc-pVQZ (H, F) and aug-cc-pV(Q+d)Z (Si,Cl) were employed while for the heavier Ge, Br, Sn and I atoms, effective core potentials embodied in the aug-cc-pVQZ-PP basis were utilized.[26-28] For the drawing of the plots, the triple-zeta homologues of the same bases were used. Finally, some Density Functional Theory (DFT) calculations with the Orca code have also been performed using the Karlsruhe def2-QZVPPD basis.[29]

Molecular energies were calculated with the Complete Active Space Self-Consistent Field (CASSCF) method[30,31] followed by Internally Contracted Multireference Configuration Interaction[32,33] plus Davidson correction with relaxed reference[34,35] (ICMRCI+Q). All the calculations were performed in C_s symmetry. The HMX molecules all have 12 valence electrons and the active space can be formed starting from the *ns* and *np* orbitals of M and X and the 1*s*,2*s*,2*p* orbitals of H. These form an active set of 13 orbitals (10a' and 3a''), which unfortunately proved to be too large for practical ICMRCI computations. The configuration space was then reduced by keeping the lowest valence a' orbital always doubly occupied and removing the two highest a' orbitals from the active space. The final active space used for the CASSCF state-averaged computations and subsequent

ICMRCI computations was then formed by 10 electrons distributed in 10 ($7a'$ and $3a''$) orbitals. The state averaged CASSCF(10,10) molecular orbitals were optimized for the three lowest electronic states of HMX: $\widetilde{X}\,^1A'$, $\widetilde{a}\,^3A''$, and $\widetilde{A}\,^1A''$.

The $\widetilde{X}\,^1A'$, $\widetilde{a}\,^3A''$ and $\widetilde{A}\,^1A''$ surfaces were mapped by means of one-dimensional plots along the HMX bending, the MH stretching and MX stretching coordinates, using the CASSCF(10,10)/ICMRCI+Q/aug-cc-pVQZ method, keeping the remaining two inactive coordinates fixed. The stationary points of the potential energy surfaces (minima for the $\widetilde{X}\,^1A'$ and $\widetilde{a}\,^3A''$ states, minimum and saddle point for the $\widetilde{A}\,^1A''$ state) for all 12 molecular species were located at the CASSCF(10,10)/ICMRCI+Q/aug-cc-pVQZ level using finite derivative methods. A grid of 5×5×5 displaced geometries was generated around the stationary points, with a spacing of 0.05 bohr for bond distances and 0.05 rad for bond angles. Single point CASSCF(10,10)/ICMRCI+Q/aug-cc-pVQZ energies were evaluated at the displaced geometries and subsequently fitted to a quartic polynomial by means of the SURFIT program.[36] The quartic polynomial was then converted to a quartic force field in internal coordinates, which was finally used to calculate the spectroscopic parameters and anharmonic vibrational levels using second order perturbation theory.[37] Equilibrium geometries, fundamental frequencies and electronic excitation energies as well as other spectroscopic information (quartic force fields, rotational constants, centrifugal distortion constants, rotation-vibration coupling constants and anharmonic vibrational constants) have been obtained for all 12 HMX molecules.

For the saddle point of the $\widetilde{A}\,^1A''$ states, a smaller grid of 3×3×3 points (with the same spacings as before) was generated and the energy fitted to a quadratic polynomial with SURFIT. This surface was used to calculate the harmonic frequencies needed to estimate the zero-point energy of the transition state.

The CASSCF(10,10) frontier orbitals (HOMO-1,HOMO,LUMO,LUMO+1) of the 12 HMX molecules were also plotted by means of the appropriate Molpro utility interfaced to the gOpenMol graphic program.[38] The geometries chosen to plot the orbitals were the same used as reference to map the potential energy surfaces.

The lowest dissociation energies of HMX were estimated by computing separately the energies of the fragments at three different level of theory: a) the density functional theory (DFT) with the Becke three parameter hybrid density functional[39] and the Lee, Yang, and Parr correlation functional[40] (B3LYP), and the def2-QZVPPD[29] basis set; b) the Complete Active Space Perturbation Theory[41,42] (CASPT2) method and c) the ICMRCI+Q technique, both b) and c) with the set of augmented quadruple-zeta bases described above and all valence electrons correlated. Basis set superposition and size consistency errors were not considered, and spin-orbit splittings and vibrational zero point energies of the diatomic products were neglected. The dissociation energies were also calculated using the supermolecule approach,[43] with the atomic and diatomic fragments placed at a collinear geometry separated by 10 Å, and optimizing the geometries of the diatomic fragments.

III. RESULTS

The most relevant parameters for our subsequent discussion of the fluorescent properties of all the HMX molecules are summarized in Tables II – IV of the manuscript. In order to explain the range and depth of the calculations that were done on each of the HMX molecules, we have elected to present the detailed results for one species and relegate the remainder to the Supplementary Material. We have chosen the molecule HGeF as our prototypical molecule, as it has some of the attributes of both the silicon and tin species and, despite considerable effort, it has never been detected by LIF methods in the gas phase.[9]

A. The electronic states of the HMX molecules

All the HMX molecules have 12 valence electrons. The four outermost electrons give the ground state configuration:

$$\widetilde{X}^1A': \ \ldots (a''_{\mathrm{HOMO-1}})^2(a'_{\mathrm{HOMO}})^2(a''_{\mathrm{LUMO}})^0(a'_{\mathrm{LUMO+1}})^0$$

As an example, the four frontier orbitals of HGeF are shown in Fig. 1, with similar plots for the other HMX species shown in the Supplementary Material. Both the a'_{HOMO} and the a''_{LUMO} are localized on the Ge atom. The former is essentially a lone-pair non-bonding sp^2 hybrid orbital while the latter is an empty p orbital. Excitation from the doubly occupied a'_{HOMO} to the unoccupied a''_{LUMO} orbital gives either a triplet state:

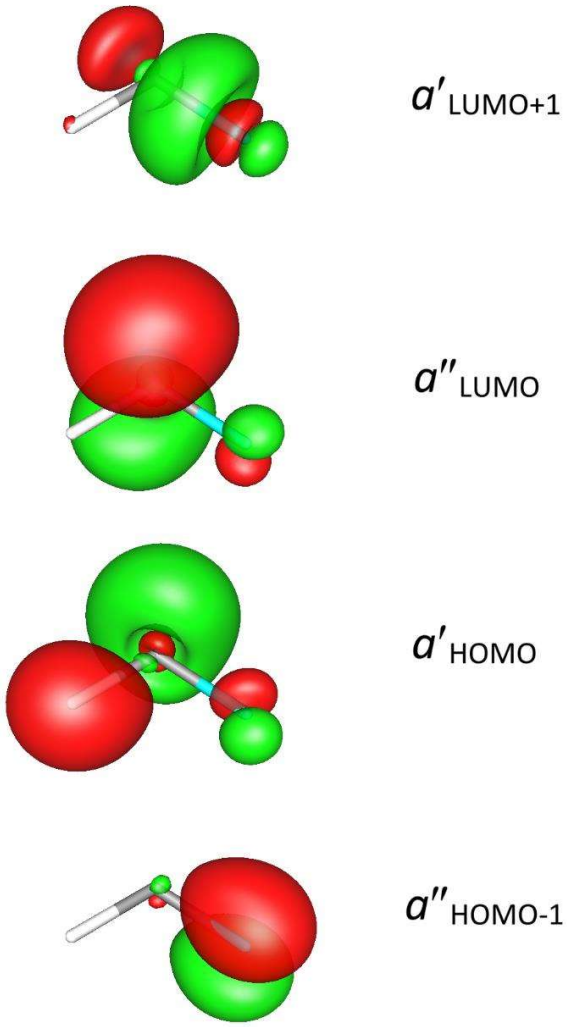

Figure 1 State-averaged CASSCF/aug-cc-pV(T+d)Z frontier molecular orbitals of HGeF. The orbitals are calculated at $r_{GeF} = 1.75$ Å, $r_{GeH} = 1.62$ Å, $\theta_{HGeF} = 100°$.

$\widetilde{a}\,^3A''$: … $(a''_{\mathrm{HOMO-1}})^2(a'_{\mathrm{HOMO}})^{\alpha}(a''_{\mathrm{LUMO}})^{\alpha}(a'_{\mathrm{LUMO+1}})^0$

or a singlet state with diradical character

$\widetilde{A}\,^1A''$: … $(a''_{\mathrm{HOMO-1}})^2(a'_{\mathrm{HOMO}})^{\alpha}(a''_{\mathrm{LUMO}})^{\beta}(a'_{\mathrm{LUMO+1}})^0$

Other excited states with A' symmetry can be produced by excitation of an electron from the doubly occupied a'_{HOMO} to the unoccupied $a'_{\mathrm{LUMO+1}}$ orbital:

$3^1A'$ …$(a''_{\mathrm{HOMO-1}})^2(a'_{\mathrm{HOMO}})^{\alpha}(a''_{\mathrm{LUMO}})^0(a'_{\mathrm{LUMO+1}})^{\beta}$

$2^3A'$: …$(a''_{\mathrm{HOMO-1}})^2(a'_{\mathrm{HOMO}})^{\alpha}(a''_{\mathrm{LUMO}})^0(a'_{\mathrm{LUMO+1}})^{\alpha}$

Potential energy curves for the low-lying electronic states of HGeF as functions of the geometric parameters are shown in Fig. 2, panels A-C. It is evident (panel A) that, for the $\widetilde{A}\,^1A''$ state along the r_{GeH} coordinate, a small barrier to dissociation is present. Such a barrier is not present either in the ground state or in the first triplet state. Moreover, the ground $\widetilde{X}^1A'$ state was found to correlate at linear geometries with a $^1\Sigma^+$ state while the $\widetilde{A}\,^1A''$ and $3^1A'$ states correlate with a $^1\Pi$ state. On the other hand, the $\widetilde{a}\,^3A''$ and $2^3A'$ triplet states correlate at linearity with a $^3\Pi$ state (panel C). This behavior is quite different from that of the HCX (X = F,Cl,Br,I) halocarbenes[44], for which the $\widetilde{X}^1A'$ and $\widetilde{A}\,^1A''$ states correlate at linear geometries with a $^1\Delta$ state.

All the HMX molecules generate similar plots as documented in the Supplementary Material. It is evident that the strongly bound $\widetilde{X}^1A'$ and $\widetilde{a}\,^3A''$ states do not show any barrier to dissociation, while the more weakly bound $\widetilde{A}\,^1A''$ states show a small barrier whose height decreases on passing from F-containing molecules to Cl-containing molecules, becoming very small or negligible for Br- and I-containing molecules. This behavior is common to all HMX, including M = carbon.[45-47]

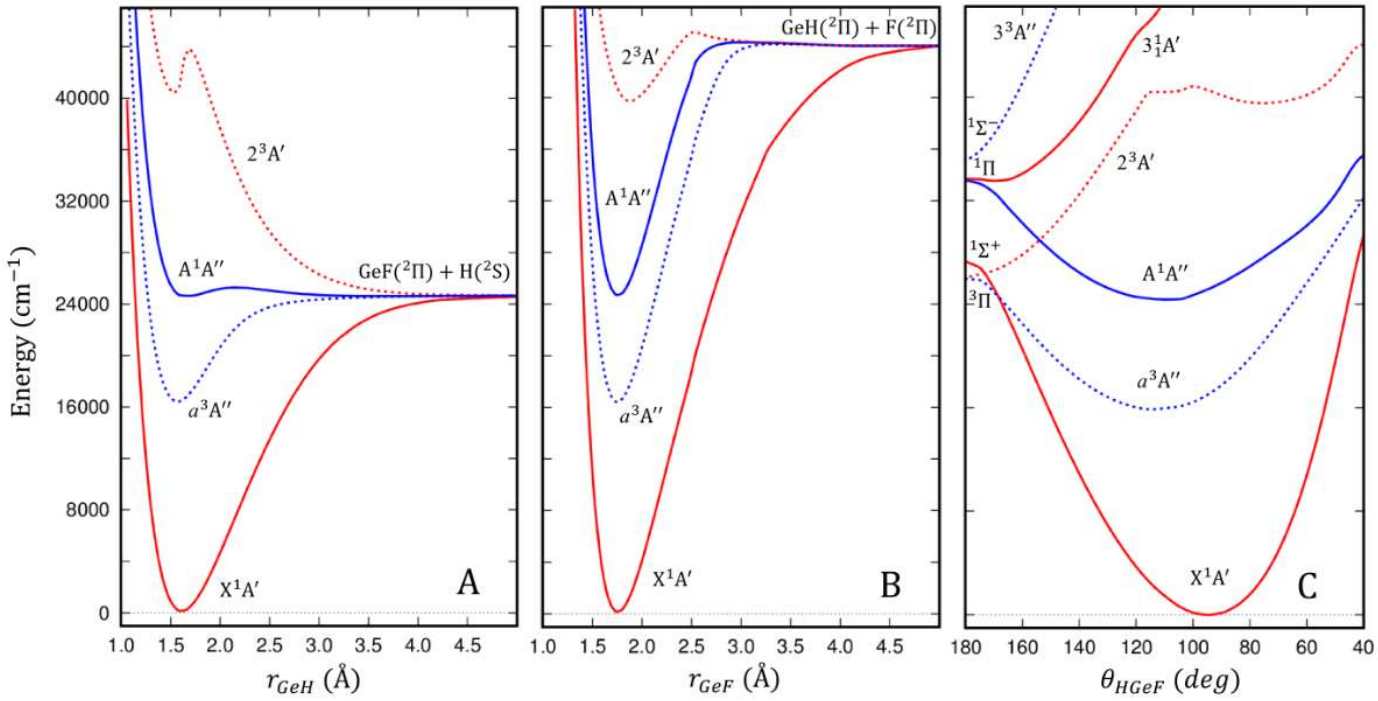

Figure 2. Low-lying singlet (solid lines) and triplet (dashed lines) potential energy curves of HGeF. Red lines correspond to A' states and blue lines to A'' states. Panel A: $r_{GeF} = 1.75$ Å, $\theta_{HGeF} = 100°$; panel B: $r_{GeH} = 1.62$ Å, $\theta_{HGeF} = 100°$; panel C: $r_{GeF} = 1.75$ Å, $r_{GeH} = 1.62$ Å; All energies are relative to the minimum of the X^1A' state

B. Dissociation products

The HMX triatomic molecules can dissociate into three different ground state atomic-diatomic products. These are

$$\begin{array}{ll} a) & MX(^2\Pi) + H(^2S) \\ b) & MH(^2\Pi) + X(^2P) \\ c) & HX(^1\Sigma^+) + M(^3P) \end{array} \qquad (1)$$

Channels a) and b) are both accessible from all three $\widetilde{X}^1A'$, $\widetilde{a}^3A''$ and $\widetilde{A}^1A''$ electronic states while spin restrictions limit channel c) to the $\widetilde{a}^3A''$ state. The relative energies, with $MX(^2\Pi) + H(^2S)$ taken as reference, of channels b) and c) have been calculated at three levels of theory, B3LYP/def2—QZVPPD, CASPT2/aug-cc-pVQZ and ICMRCI+Q/aug-cc-pVQZ. These relative energies correspond to the differences between the dissociation energies of the MX and the MH diatomic molecules and to the differences between the dissociation energies of MX and HX diatomic molecules, respectively. The results are summarized in Table I and compared with the values obtained from tabulated experimental dissociation energies.[48] For the ICMRCI+Q method, a second value enclosed in square parentheses is also reported in Table I,. This quantity was evaluated as the difference in the dissociation energies reported in Tables II-IV, which in turn were obtained with the supermolecule approach. The various methods give relative energies which can differ by as much as ~7000 cm^{-1} (~ 80 kJ/mol) reflecting the intrinsic difficulty of obtaining accurate thermochemical predictions by means of *ab initio* methods. By comparing the theoretical and experimental values, it is evident that none of the four methods is noticeably better than the others. However, the CASPT2 and supermolecule ICMRCI values are generally closest to each other. On the other hand, the experimental values themselves are subject to large errors, making comparisons quite awkward. Despite these difficulties, some general trends can be recognized. First, the $HX(^1\Sigma^+) + M(^3P)$ dissociation is always the energetically most favorable, but only the $\widetilde{a}^3A''$ state of HMX can dissociate in this way. The $\widetilde{X}^1A'$ and $\widetilde{A}^1A''$ states, having different spin multiplicity, can access this dissociation channel only through an intersystem crossing to the $\widetilde{a}^3A''$ state. Second, the $MH(^2\Pi) + X(^2P)$ halogen loss dissociation

Table I. Calculated lowest dissociative channels of the HMX species. All energies (in cm^{-1}) are relative to the $MX(^2\Pi) + H(^2S)$ channel. Calculations are performed at the B3LYP/def2-QZVPPD (upper value) CASPT2/aug-cc-pVQZ (middle value) and ICMRCI+Q/aug-cc-pVQZ (lowest value) levels. The value enclosed in square parentheses on the same line of ICMRCI+Q is evaluated from the dissociation energies reported in Tables II-IV. The values reported in parentheses for the $HX(^1\Sigma^+) + M(^3P)$ channels are the difference between the experimental MX and HX diatomic dissociation energies. The values reported in parentheses for the $MH(^2\Pi) + X(^2P)$ channels are the difference between the experimental MX and MH diatomic dissociation energies. All experimental dissociation energies taken from ref. 48. See text for details.

		F	Cl	Br	I
HSiX	$HX(^1\Sigma^+) + Si(^3P)$	693 -617 -1703 (600±1400)	-1707 -1896 -3474 (-1230±530)	-1481 -918 -2246 (-670±720)	-1687 -372 -1560 (-4610±710)
	$SiH(^2\Pi) + X(^2P)$	23178 23617 21133 [23571] (23700±1600)	7233 10234 8131 [9248] (10320±690)	4530 5581 3633 [4786] (5430±860)	-330 836 -1134 [70] (-4200±860)
HGeX	$HX(^1\Sigma^+) + Ge(^3P)$	-5478 -6388 -7275 (-3900±1100)	-4122 -4509 -5986 (-3400±800)	-3102 -2817 -4139 (-1600±690)	-2653 -1707 -2913 (-2500±2100)
	$GeH(^2\Pi) + X(^2P)$	18894 19797 17873 [22678] (21700±1500)	8332 9571 7732 [9288] (10700±1200)	4796 5622 3853 [5356] (7000±1100)	591 1451 -374 [1366] (400±2500)
HSnX	$HX(^1\Sigma^+) + Sn(^3P)$	-8038 -9272 -10286 (-7800±670)	-5325 -5818 -7303 (-6800±670)	-3964 -4344 -5734 (-2400±1100)	-3300 -3284 -4682 (-5290±260)
	$SnH(^2\Pi) + X(^2P)$	24312 18863 16669 [19016] (17700±2100)	9210 10113 8422 [11571] (7200±2100)	6014 6056 4265 [7613] (6100±2500)	2024 1825 -137 [1908] (-2400±1700)

generally requires more energy than the $MX(^2\Pi) + H(^2S)$ hydrogen loss dissociation. However, the difference decreases rapidly going from F to Cl to Br, and for HMI compounds in the $\tilde{A}\ ^1A''$ state, the halogen loss dissociation may be competitive with hydrogen loss. This fact and the presence of a secondary minimum in the $\tilde{A}\ ^1A''$ potential energy surfaces make predictions for the HMI compounds particularly difficult.

C. Spectroscopic properties of HMX ground and lowest excited states

Tables II -IV summarize the major results of this study, with each cell containing the calculated value and an experimental value (where available) directly below in parentheses. First the calculated geometric parameters of each molecule are tabulated along with any available experimentally determined values. Since *the* $\tilde{a}\ ^3A''$-$\tilde{X}\ ^1A'$ transitions have yet to be observed for any of the HMX molecules, there are no experimental data available for the triplet states. The *ab initio* values are equilibrium values (r_e) whereas the experimental quantities are usually zero-point (r_0) values, which would be expected to be slightly larger. HGeF and DGeF and many of the HSnX species have not been detected spectroscopically so there is no experimental information on their geometries, vibrational frequencies or electronic excited states. For each species we also report the geometry and energy of the transition state ($\tilde{A}_{TS}$) connecting the $\tilde{A}$ state minimum to the dissociation limit and the energies of the dissociation limits for the MX + H and MH + X channels. The latter, calculated at the same level as the equilibrium energies, were computed within the supermolecule approach.

In column 6 ("Energy") the calculated T_e energies are reported relative to the minimum of the $\tilde{X}$ state. The next entries in the Tables are the vibrational *fundamentals* with ν_1 = MH stretch, ν_2 = bend and ν_3 = MX stretch. These have been calculated by determining the harmonic vibrational frequencies and anharmonicities and combining them with the relationships:

$$v_1 = \omega_1 + 2x_{11} + \frac{1}{2}(x_{12} + x_{13}) \qquad (2)$$

$$v_2 = \omega_2 + 2x_{22} + \frac{1}{2}(x_{21} + x_{23}) \qquad (3)$$

Table II. Spectroscopic parameters for the $\tilde{X}$, $\tilde{a}$ and $\tilde{A}$ states of HSiX, and DSiX (X = F, Cl, Br, I). Experimental data (in parentheses) from refs. 1-8. See the text for other details.

Molecule	State	Geometry (Å, deg)			Energy	HSiX				DSiX				Predicted Emission Properties			
						Fundamentals (cm^{-1})			Energy (cm^{-1})	Fundamentals (cm^{-1})			Energy (cm^{-1})	Max energy (cm^{-1})		Max v_2'	
		r_{SiX}	r_{SiH}	Θ_{HSiX}	T_e	ν_1	ν_2	ν_3	T_0	ν_1	ν_2	ν_3	T_0	HSiX	DSiX	HSiX	DSiX
HSiF	$\tilde{X}$	1.622 (1.606)	1.527 (1.548)	96.5 (97.0)	-	1947 (1932)	885 (860)	806 (838)	-	1413 (1401)	637 (638)	833 (840)	-				
	$\tilde{a}$	1.618	1.489	115.4	13697	2064	611	850	13634	1518	452	834	13652				
	$\tilde{A}$	1.619 (1.602)	1.528 (1.557)	117.5 (114.4)	23699	1639 (1547)	536 (558)	835 (857)	23406 (23260)	1231 (1174)	395 (425)	823 (854)	23493 (23339)	2945 (2398)	3223 (2792)	4 (4)	6 (6)
	$\tilde{A}_{TS}$	1.623	2.340	88.3	27693	382i	194	831	26351	280*i*	146	831	26716				
SiF+H		1.609	10	180	26304												
SiH+F		10	1.521	180	49875												
HSiCl	$\tilde{X}$	2.078 (2.073)	1.518 (1.521)	95.4 (95.0)	-	1961 (1969)	801 (806)	515 (523)	-	1423 (1434)	584 (592)	515 (518)	-				
	$\tilde{a}$	2.049	1.483	115.6	11992	2066	641	548	11989	1503	465	554	11996				
	$\tilde{A}$	2.051 (2.047)	1.509 (1.505)	117.8 (116.5)	21021	1776 (1747)	564 (564)	532 (532)	20852 (20718)	1308 (1301)	413 (409)	535 (543)	20906 (20773)	4732 (3761)	5050 (4106)	9 (4)	12 (10)
	$\tilde{A}_{TS}$	2.075	2.458	87.1	26915	338i	164	521	25584	-243*i*	120	521	25956				
SiCl+H		2.068	10	180	26795												
SiH+Cl		10	1.522	180	36043												
HSiBr	$\tilde{X}$	2.248 (2.237)	1.517 (1.518)	94.5 (93.4)	-	1952 (1976)	761 (772)	410 (412)	-	1406 (1440)	550 (562)	410 (408)	-				
	$\tilde{a}$	2.214	1.485	115.9	11711	2047	603	435	11698	1477	441	433	11706				
	$\tilde{A}$	2.219 (2.208)	1.509 (1.497)	117.9 (116.4)	20177	1794 (1787)	529 (535)	417 (417)	20014 (19903)	1308 (1326)	385 (376)	417 (434)	20064 (19954)	5317 (4972)	5642 (4307)	10 (5)	15 (8)
	$\tilde{A}_{TS}$	2.242	2.589	83.7	26646	252i	146	416	25331	179*i*	107	415	25706				
SiBr+H		2.233	10	180	26650												
SiH+Br		10	1.522	180	31436												
HSiI	$\tilde{X}$	2.477 (2.463)	1.517 (1.534)	93.3 (92.4)	-	1952 (1983)	715 (727)	349 (350)	-	1402 (1443)	514 (528)	349 (345)	-				
	$\tilde{a}$	2.432	1.487	116.5	11021	2041	573	370	11010	1469	413	371	11017				
	$\tilde{A}$	2.441 (2.436)	1.507 (1.515)	117.7 (114.9)	18635	1842 (1853)	492 (485)	344 (336)	18490 (18259)	1336 -	359 (368)	343 (325)	18534 (18303)	6616 (3115)	6964 (2650)	>6 (4)	>10 (4)
	$\tilde{A}_{TS}$ [a]	2.455	10	180	26476	0	0	344 [b]	25106	0	0	343 [b]	25498				
SiI+H		2.455	10	180	26476												
SiH+I		10	1.521	180	26546												

[a] No barrier was found along the SiI + H dissociation channel for the $\tilde{A}$ state of HSiI. For consistency with the other entries of this Table, the geometry and energy of the SiI+H limit is reported.

[b] Assumed equal to ν_3 of the $\tilde{A}$ state. This value is used to estimate ZPE.

Table III. Spectroscopic parameters for the $\widetilde{X}$, $\widetilde{a}$ and $\widetilde{A}$ states of HGeX, and DGeX (X = F, Cl, Br, I). Experimental data (in parentheses) from refs. 9-12. See the text for other details.

Molecule	State	Geometry			Energy	HGeX				DGeX				Predicted Emission Properties			
						Fundamentals (cm^{-1})			Energy (cm^{-1})	Fundamentals (cm^{-1})			Energy	Max Energy (cm^{-1})		Max v_2'	
		r_{GeX}	r_{GeH}	Θ_{HGeX}	T_e	v_1	v_2	v_3	T_0	v_1	v_2	v_3	T_0	HGeX	DGeX	HGeX	DGeX
HGeF	$\tilde{X}$	1.764	1.604	94.2	-	1879	792	627	-	1375	536	675	-				
	$\tilde{a}$	1.753	1.558	116.1	15885	1819	526	668	15774	1351	386	663	15808				
	$\tilde{A}$	1.759	1.640	114.6	24382	925	379	643	23859	767	285	632	24012	386 [a]	564 [a]	1 [a]	1 [a]
	$\tilde{A}_{TS}$	1.767	2.162	90.9	25473	402*i*	219	645	24245	296*i*	160	645	24576				
GeF+H		1.765	10	180	25165												
GeH+F		10	1.599	180	47843												
HGeCl	$\tilde{X}$	2.193 (2.176)	1.599 (1.594)	93.8 (95.3)	-	1832 (1830)	724 (721)	393 (400)	-	1330 (1320)	527 (521)	390 (398)	-				
	$\tilde{a}$	2.156	1.557	114.5	14384	1850	562	411	14340	1352	433	389	14358				
	$\tilde{A}$	2.166 (2.146)	1.608 (1.613)	115.0 (114.5)	21950	1324 (1263)	445 (431)	389 (399)	21634 (21515)	1005 (980)	324 (322)	397 (399)	21730 (21614)	1700 (1218)	1950 (1533)	3 (2)	6 (4)
	$\tilde{A}_{TS}$	2.190	2.325	84.9	24565	326*i*	148	403	23334	234*i*	107	403	23680				
GeCl+H		2.181	10	180	24467												
GeH+Cl		10	1.598	180	33753												
HGeBr	$\tilde{X}$	2.346 (2.326)	1.597 (1.613)	93.5 (94.1)	-	1823 (1835)	699 (694)	289 (291)	-	1313 (1322)	502 (498)	288 (290)	.				
	$\tilde{a}$	2.307	1.559	114.9	13957	1843	536	301	13908	1337	388	300	13926				
	$\tilde{A}$	2.324 (2.308)	1.604 (1.615)	115.2 (116.3)	21264	1407 (1381)	428 (419)	280 (280)	20977 (20660)	1047 (1048)	315 (312)	279 (279)	21064 (20746)	2201 (1727)	2463 (2185)	5 (3)	8 (4)
	$\tilde{A}_{TS}$	2.333	2.533	81.5	24394	235*i*	135	304	23178	167*i*	97	304	23527				
GeBr+H		2.325	10	180	24430												
GeH+Br		10	1.598	180	29786												
HGeI	$\tilde{X}$	2.565 (2.525)	1.596 (1.593)	92.5 (93.5)	-	1825 (1839)	663 (661)	234	-	1311 -	474 (473)	234 (239)	-				
	$\tilde{a}$	2.517	1.560	115.5	13130	1856	513	243	13089	1341	369	242	13104				
	$\tilde{A}$ [b]	2.544 (2.515)	1.596 (1.618)	114.6 (116.2)	19678	1540 (1542)	386 (337)	213 (203)	19435 (18929)	1130 (1144)	283 (260)	214 (205)	19507 (19002)	3528 (1811)	3821 (1144)	9 (2)	14 (2)
	$\tilde{A}_{TS}$ [c]	2.558	2.806	81.5	24246	0	0	213 [d]	22963	0	0	214 [d]	23328	-	-	-	.
GeI+H		2.529	10	180	24379												
GeH+I		10	1.599	180	25745												

[a] No fluorescence detected

[b] A secondary minimum at r_{GeI}=2.712 Å, r_{GeH}=1.719 Å, Θ_{HGeI}=57.9° was found. The energy of the secondary minimum is at 19896 cm^{-1} above the ground state minimum (218 cm^{-1} above the main minimum of $\tilde{A}$). The transition state connecting the secondary minimum to the main minimum is at r_{GeI}=2.628Å, r_{GeH}=1.646Å, Θ_{HGeI}=82.9°, with energy T_e=20523 cm^{-1} above the ground state (845 cm^{-1} above the main minimum of $\tilde{A}$)

[c] Very shallow transition state. The harmonic frequencies were not calculated.

[d]. Assumed equal to ν_3 of the $\tilde{A}$ state. This value is used to estimate ZPE

Table IV. Spectroscopic parameters for the $\widetilde{X}$, $\widetilde{a}$ and $\widetilde{A}$ states of HSnX, and DSnX (X = F, Cl, Br, I). Experimental data (in parentheses) from ref. 13. See the text for other details.

Molecule	State	Geometry				HSnX				DSnX				Predicted Emission Properties			
						Fundamentals (cm^{-1})			Energy	Fundamentals (cm^{-1})			Energy	Max Energy		Max v_2'	
		r_{SnX}	r_{SnH}	Θ_{HSnX}	T_e	ν_1	ν_2	ν_3	T_0	ν_1	ν_2	ν_3	T_0	HSnX	DSnX	HSnX	DSnX
HSnF	$\tilde{X}$	1.962	1.790	92.9	-	1664	654	533	-	1227	425	594	-				
	$\tilde{a}$	1.952	1.746	114.9	15484	1624	412	586	15385	1204	306	582	15416				
	$\tilde{A}$	1.959	1.858	113.1	23102	568	250	558	22529	529	197	538	22696	-14	110	0	0
	$\tilde{A}_{TS}$	1.967	2.269	91.5	23593	347i	191	569	22515	255i	137	568	22806				
SnF+H		1.967	10	180	23348												
SnH+F		10	1.784	180	42364												
HSnCl	$\tilde{X}$	2.381	1.794	92.9	-	1685 (1665)	609 (591)	363 (349)	-	1220	448 (426)	354 (352)	-				
	$\tilde{a}$	2.351	1.754	112.2	14473	1624	459	372	14400	1189	324	383	14425				
	$\tilde{A}$	2.364	1.832	112.2	21612	918	349	342	21198 (20706)	725	247 (234)	360	21324 (20831)	466 (0)	645 (458)	1 (0)	2 (2)
	$\tilde{A}_{TS}$	2.380	2.359	88.0	22740	374i	152	390	21664	271i	109	390	21969				
SnCl+H		2.374	10	180	22524												
SnH+Cl		10	1.785	180	34095												
HSnBr	$\tilde{X}$	2.522	1.789	93.1	-	1677	612	256	0	1206	440	254	0				
	$\tilde{a}$	2.494	1.753	112.7	14048	1635	441	259	13963	1185	320	257	13990				
	$\tilde{A}$ [a]	2.510	1.816	113.5	20830	1105	342	246	20478	836	258	238	20584	1366	1577	4	6
	$\tilde{A}_{TS}$	2.487	2.608	89.4	22930	286i	116	301	21844	205i	82	301	22161				
SnBr+H		2.488	10	180	22806												
SnH+Br		10	1.785	180	30419												
HSnI	$\tilde{X}$	2.739	1.784	92.9	-	1698	601	198	-	1217	430	197	-				
	$\tilde{a}$	2.705	1.752	113.5	13293	1663	428	199	13207	1200	308	199	13233				
	$\tilde{A}$ [b]	2.733	1.799	114.2	19490	1305	338	180	19203	962	246	179	19287	2668	2920	7	12
	$\tilde{A}_{TS}$ [c]	2.686	10	180	23049	0	0	180[d]	21871	0	0	179[d]	22207				
SnI+H		2.686	10	180	23049												
SnH+I		10	1.792	180	24957												

[a] A secondary minimum at r_{SnBr}=2.795 Å, r_{SnH}=2.025 Å, Θ_{HSnBr}=39.1° was found. The energy of the secondary minimum is 21923 cm^{-1} above the ground state (1093 cm^{-1} above the main minimum of $\tilde{A}$). No transition state connecting the two minima was found

[b] A secondary minimum at r_{SnI}=2.962 Å, r_{SnH}=1.922 Å, Θ_{HSnI}=45.7° was found. The energy of the secondary minimum is 19112 cm^{-1} above the ground state (378 cm^{-1} below the main minimum of $\tilde{A}$). This is actually the global minimum of the $\tilde{A}$ potential energy surface. The transition state connecting the secondary minimum to the main minimum is at r_{SnI}=2.721 Å, r_{SnH}=1.917 Å, Θ_{HSnI}=68.1°, with energy T_e=21506 cm^{-1} above the ground state (2016 cm^{-1} above the main minimum of $\tilde{A}$).

[c] No barrier was found along the SnI + H dissociation channel for the $\tilde{A}$ state of HSiI. For consistency with the other entries of this Table, the same geometry and energy of the SnI+H limit is reported.

[d] Assumed equal to ν_3 of the $\tilde{A}$ state. This value is used to estimate ZPE

$$v_3 = \omega_3 + 2x_{33} + \frac{1}{2}(x_{31} + x_{32}) \qquad (4)$$

Anharmonic zero-point vibrational contributions at the minima of the PES's have been calculated with:

$$ZPE = \frac{1}{2}(\omega_1 + \omega_2 + \omega_3) + \frac{1}{4}(x_{11} + x_{22} + x_{33} + x_{12} + x_{12} + x_{23}) \quad (5)$$

For the transition states, the zero-point vibrational correction has been calculated using only the harmonic frequencies, excluding the imaginary vibrational frequency from the sum. In Tables II-IV only the fundamentals are reported, relegating the harmonic frequencies, anharmonic constants and other spectroscopic quantities to the Supplementary Material.

The calculated fundamentals can be readily compared to experiment since $v_1 = 1_0^1 - 0_0^0$ etc. Similar calculations are reported for the DMX molecules which are usually studied experimentally in tandem with the hydrogenated species. The triplet state theoretical results will be useful in future attempts to detect the laser induced phosphorescence (LIP) spectra.

Combining the *ab initio* electronic energy differences and zero-point energies yielded the calculated T_0 values for comparison with experiment as shown in columns 10 (HMX) and 14 (DMX) of the Tables. These T_0 values compare favorably with experiment (where data are available), typically 100-200 cm^{-1} too high for the HSiX molecules and 300-500 cm^{-1} too high for HGeX. Such systematic deviations may be due both to intrinsic limitations of the electron correlation treatment and to the finite size of the basis sets, in addition to the use of pseudopotentials for Ge atoms (the $\tilde{X} - \tilde{A}$ transitions involve orbitals mainly localized on the central atom). Similar deviations (300 – 500 cm^{-1}) are then expected for Sn-containing molecules

The final four columns of Tables II-IV concern the predicted fluorescence properties of the HMX molecules. Under the Max. Energy heading, we have tabulated the energy difference between the ZPE-corrected energy barrier to dissociation of the $\widetilde{A}$ state and the zero-point energy of the $\widetilde{A}$ state. This quantity provides an upper limit to the energy range of the vibrational levels in the $\widetilde{A}$ state that are below the barrier to dissociation and therefore can potentially fluoresce back down to the ground state. These numbers are different for HMX and

DMX, due to the lower zero-point energy of the DMX species. For the experimental counterpart, we report the vibrational energy of the highest observed level in the LIF spectrum. There are no entries in the triplet state row since the $\tilde{a}$ state potentials have deep wells (see for example, Fig, 2 for HGeF) and would all be expected to phosphoresce if the weak spin-forbidden transitions could be observed and the Franck-Condon factors were favorable.

Transitions to the upper state bending levels predominate in the experimentally observed LIF spectra, a direct consequence of the large increase in the bond angle on electronic excitation. With this in mind, an alternative measure of the extent of the LIF spectrum is to count the number of bands expected in the bending progression (2_0^1, 2_0^2, etc.) before the onset of dissociation, which can be readily compared with experiment. These results are presented in the columns labelled Max v_2', with larger values for DMX again due to the difference in zero-point energies.

It is important to emphasize that both Max Energy and Max v_2' are the calculated *Maximum* energy and v_2' quantum number predicted for the LIF spectrum. There are at least three factors that may be responsible for lowering these values in real experimental results. First, the Franck-Condon factors may mitigate against observing transitions high up in the excited state vibrational manifold. Second, there may be experimental reasons why the observed LIF spectrum is weak such as inefficient laser dyes or poor production of the HMX molecules in our discharge jet,[6-12] so that the transitions to higher levels were not observed. Third, tunneling through the dissociation barrier may occur, so that our numbers may overestimate the extent of the LIF band system for some HMX species.

D. $\tilde{A}\,^1A''$ state well depths and energy barriers to dissociation

From the energies reported in the T_e column of tables II-IV it is possible to analyze the energy barriers to dissociation of the $\tilde{A}$ states (without vibrational contribution) as the sum of two terms, each one referred to the MX + H dissociation limit: the depth of the potential energy well and the height of the transition state. These values are plotted in Fig.3. From the figure it is evident that, for each M atom, the depth of the potential well

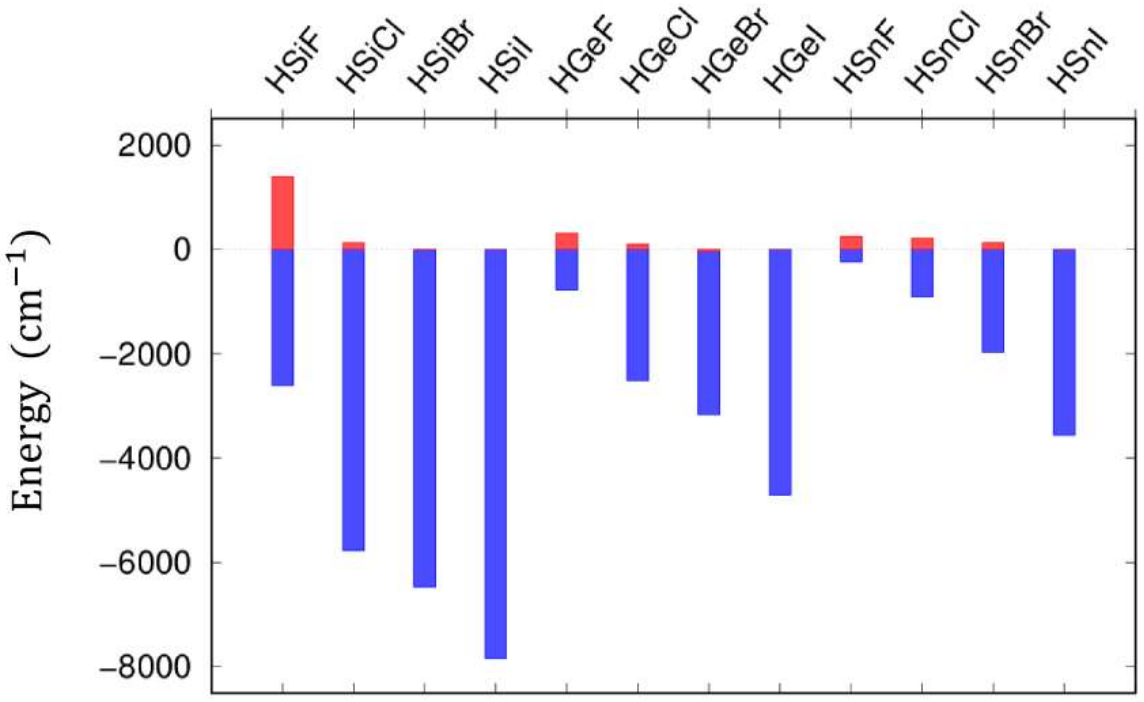

Figure 3. MX + H dissociation energies from the $\widetilde{A}\,^1A''$ excited state of HMX. The depth of the bonding well with respect to the dissociation limit is shown in blue, the height of the dissociation barrier above the dissociation limit is in red.

increases regularly from F to I along the halogen series, while for each halogen it decreases smoothly from Si to Sn. On the other hand, the height of the transition state is relevant only for fluorine compounds and, to a much less extent, for chlorine compounds, being essentially zero for the bromine- and iodine-containing molecules.

IV. DISCUSSION

A. Rationale for trends in the $\tilde{A}$ state well depth and barriers to HMX → H + MX dissociation

Our calculations show that some HMX molecules have a significant $\tilde{A}$ state energy barrier to the H + MX dissociation (see Tables II-IV and Fig. 3) whereas there is no barrier evident in the $\tilde{X}$ or $\tilde{a}$ states and the $\tilde{A}$ state bonding potential wells vary systematically with the identity of the halogen. Here we attempt to rationalize these findings based on the relevant potential energy curves, similar to the approach used in a previous study of the isoelectronic HNO free radical.[49] We start by considering the potential curves for the linear HGeX molecules as a function of the H-Ge bond distance as shown in Fig. 4. It is evident that the major difference among the various species is the behavior of the $^1\Delta$ state, with high dissociation asymptote for HGeF, becoming progressively lower through HGeCl, HGeBr and HGeI. Similar calculations show that the same trends are found for the HSiX and HSnX molecules.

For linear geometries the $^1\Sigma^+$, the $^3\Sigma^-$ and the $^1\Delta$ states are strongly bound and correlate asymptotically along the r_{GeH} stretching coordinate with the excited GeF products H(^{2}S) + GeF($A^2\Sigma^+$), H(^{2}S) + GeF($a^4\Sigma^-$) and H(^{2}S) + GeF($C^2\Delta$), respectively, whereas the $^1\Pi$ and $^3\Pi$ states are either dissociative or weakly bound and correlate with the ground state H(^{2}S) + GeF($X^2\Pi$) products. In linear configurations, all these electronic states have different symmetry, so there is no interaction between them (ignoring spin orbit coupling), which leads to curve crossings between all the states.

As the molecule bends, it assumes C_s symmetry and the degeneracies of the electronic states are lifted forming species of A' and A'' symmetry. The doubly degenerate $^1\Pi$ and $^1\Delta$ states split into two components, one

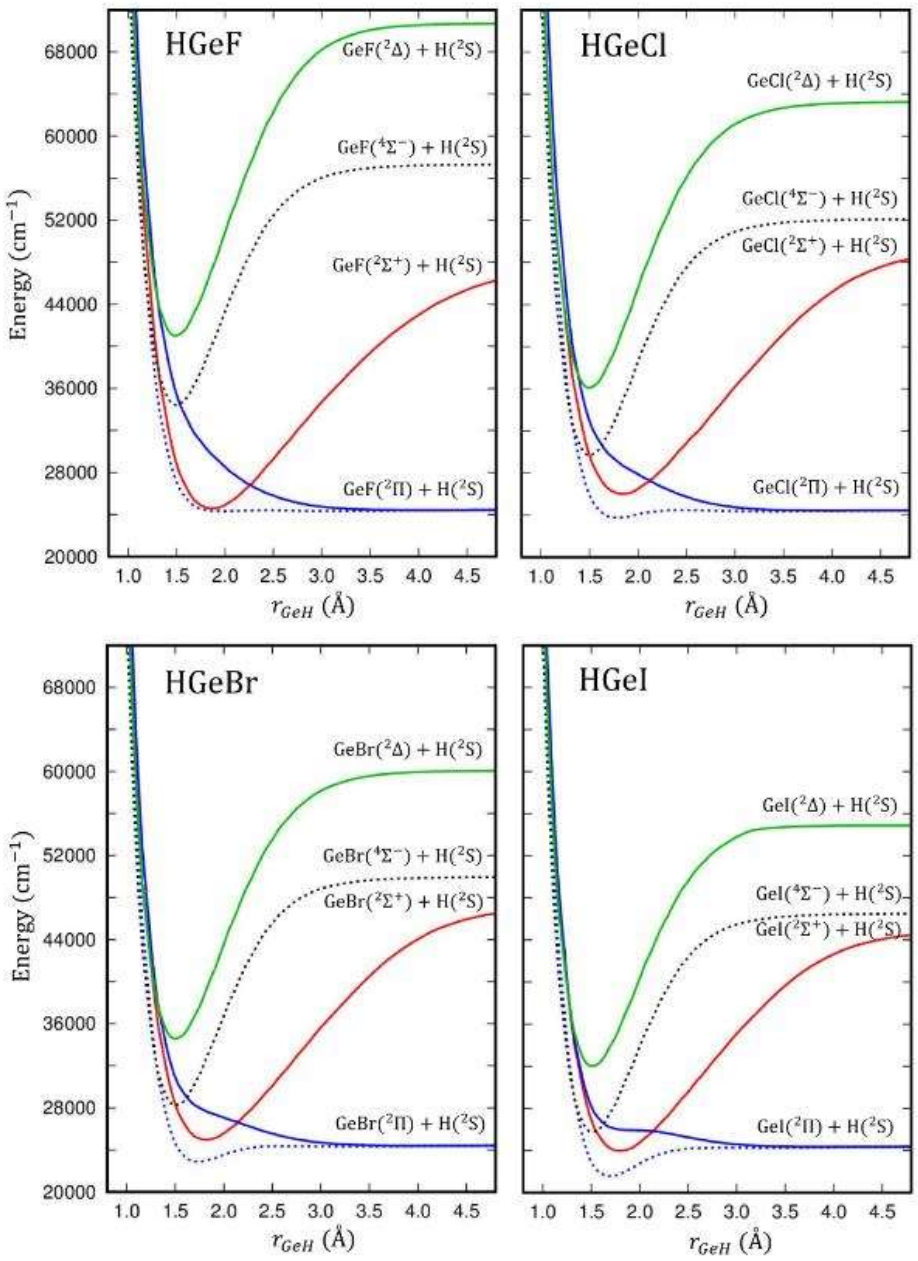

Figure 4. Linear molecule HGeX potential energy curves as a function of GeH bond distance. Singlet states are denoted by solid lines and triplet states by dashed lines. Red lines are Σ^+ states, blue lines Π states, black lines Σ^- states and green lines Δ states.

with $^1A'$ and the other with $^1A''$ symmetry, as shown by the correlation diagram in Fig. 5. The strongly bound $^1\Sigma^+(^1A')$ and $^1\Delta$ $(^1A')$ states mix with the repulsive $^1\Pi$ $(^1A')$ state to form the bound $\tilde{X}^1A'$ state. Similarly, the strongly bound $^3\Sigma^-(^3A'')$ state mixes with the weakly bound $^3\Pi$ $(^3A'')$ state to form the bound $\tilde{a}^3A''$ state. In both the $\tilde{X}^1A'$ and $\tilde{a}^3$A" states, the attractive Σ (and Δ) character prevails over the repulsive Π character at all geometries, eliminating any barrier to dissociation for all HMX molecules.

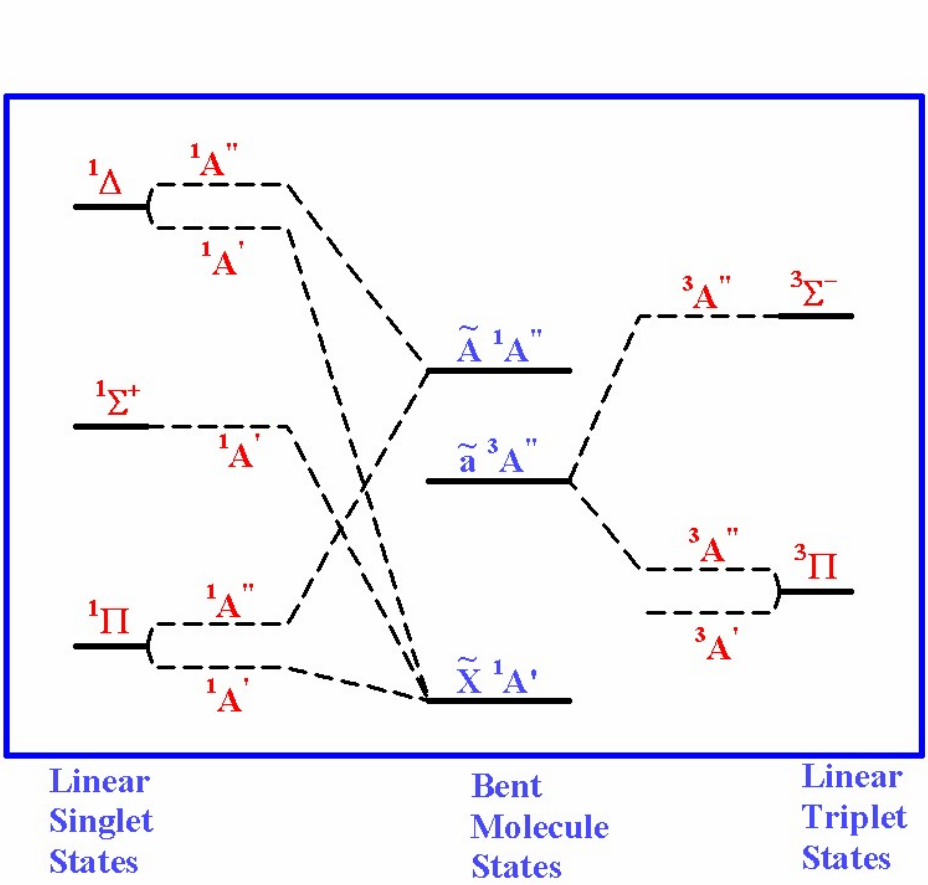

Figure 5. Correlation diagram of the linear HMX molecule singlet and triplet states with the bent molecule states. The higher energy bent molecule ^{3}A′ states are not shown.

The situation is more complicated for the $\widetilde{A}\,^1A''$ state, which is formed by the mixing of the $^1A''$ components of the $^1\Delta$ and $^1\Pi$ states on bending. The attractive nature of this state at intermediate values of r_{GeH} reflects the dominant $^1\Delta$ character, with a switch to the repulsive $^1\Pi$ character at large r_{GeH} values. The depth of the bonding well and the height of any barrier to dissociation in the $\widetilde{A}\,^1A''$ state is then governed by a delicate balance between the opposing effects of the depth of the $^1\Delta$ attractive well and the repulsive nature of the $^1\Pi$ state. For the fluorinated molecules (HMF), the $^1\Delta$ lies at higher energies (compared to other halogens) and the $^1\Pi$ state contribution dominates, yielding a significant barrier to dissociation and a small bonding well. Progressing through the halogens, the $^1\Delta$ state lowers and gets closer to the $^1\Pi$ state becoming increasingly dominant, so the $\widetilde{A}$ state bonding depth increases and overwhelms the barrier to dissociation (see Fig. 3).

In other words, the shape of the $\widetilde{A}$ state potential is the result of a strong avoided crossing between the A'' component of the repulsive $^1\Pi$ ground state and the A'' component of the attractive $^1\Delta$ excited state. If the interaction (occurring only at bent geometries) between these states is weak, the $\widetilde{A}$ state remains essentially dissociative (HSnF, for example). If it is strong, the state became fully attractive and the barrier eventually disappears (contrast HSnI with HSnF in Fig. 3).

B. The $\widetilde{X}^1A'$ ground states

All of the HSiX ground state species have been characterized spectroscopically and our theoretical results are in good agreement with experiment. A careful study of Table II shows maximum deviations (|obs. – calc.|) in bond lengths of 0.021 Å (HSiF), bond angles of 1.1 ° (HSiBr) and vibrational fundamentals of 41 cm^{-1} (DSiI). For HGeX, the HGeF species has not been observed experimentally, although the others have been studied by LIF and wavelength resolved emission studies. Table III shows maximum deviations (|obs. – calc.|) in bond lengths of 0.04 Å (HGeI), bond angles of 1.5 ° (HGeCl) and vibrational fundamentals of 14 cm^{-1} (HGeI). HSnCl is the only HSnX species currently known experimentally and the maximum deviation in the ground state

fundamentals (Table IV) is 20 cm^{-1}. The trends indicate that our theoretical values for the experimentally unknown HMX ground state quantities should be similarly reliable.

C. The $\tilde{a}\,^3A''$ states

None of the triplet states of the HMX species have been observed experimentally so the values in Tables II – IV provide predictions for future studies. All the triplet states have deep bonding wells supporting a broad range of vibrational levels, no barrier to the H + MX dissociation, and a large bond angle relative to the ground state. The HSiX $\tilde{a}$ - $\tilde{X}$ transitions are quite low in energy [T_0 = 732 nm (HSiF) to 908 nm (HSiI)] and are liable to be quite weak, making them difficult to detect. The progression to HGeX and HSnX shifts the $\tilde{a}$ - $\tilde{X}$ transitions 1000 – 2000 cm^{-1} to higher energy and the increase in spin-orbit coupling should make the triplet-singlet transitions more intense. The large change in bond angle indicates that long Franck-Condon active progressions in the bending mode would be expected in LIP spectra accompanied by a significant increase in the A rotational constant on excitation.

D. Fluorescence properties of the HMX $\tilde{A}\,^1A''$ states

The main results obtained from this systematic study of HMX compounds concern the fluorescence properties of the $\tilde{A}$ states and predictions of whether and/or to what extent the individual species can be detected by LIF spectroscopy. We discuss each molecule individually.

HSiF. The $\tilde{A}$ state has quite a high barrier to dissociation (≈1400 cm^{-1}, the highest within the molecules considered here) and a well-developed bonding potential well (≈ -2600 cm^{-1}). The predicted emission properties match experiment very well, both for the fluorescence energy interval and for the number of observable bending levels. For both isotopologues, the experimental LIF spectrum stops about 500 cm^{-1} below the theoretical maximum. The calculated HSiF absorption spectrum[50] shows that the major 2_0^n progression peaks at 2_0^2 and becomes very weak beyond 2_0^4 or 2_0^5, depending on the level of theory, in good agreement with experiment and the present theoretical predictions.

HSiCl. With respect to HSiF, the barrier to dissociation is drastically lowered to 120 cm^{-1} but the bonding well depth is approximately doubled. This leads to a near-doubling of the fluorescence energy interval and of the bending levels within this interval, although the experimental results stop well short of these theoretical maxima. The calculated absorption spectra[16] of HSiCl and DSiCl show that the Franck-Condon activity fades away about 4000 cm^{-1} above the 0-0 band, with Max $v_2' = 4$ for HSiCl and 10 for DSiCl, in excellent accord with experiment. It is evident that with the increased well-depth, the extent of the observed LIF spectrum is Franck-Condon rather than dissociation limited.

HSiBr. For this species the dissociation barrier becomes negligible but the bonding well depth is further lowered to ≈ 6500 cm^{-1} below the SiBr + H dissociation limit. Theory predicts that up to 10 (15) bending levels might be observed for HSiBr (DSiBr), but experimental observations stop at about half of the theoretical maximum number, again due to the lack of Franck-Condon activity.

HSiI. No barrier to dissociation was found and the bonding well is ≈ 7800 cm^{-1}, the deepest of the whole HMX series. In spite of this, the number of observed bending levels is only about half of that predicted theoretically, a consequence of at least two mitigating factors. First, Franck-Condon considerations probably limit the observable extent of the LIF spectrum to 3000 – 4000 cm^{-1}. Second, the observed LIF spectra of HSiI and HGeI are characterized as weak[7,12] so they may not span the full range of bands. In our experiments, these species were synthesized by subjecting H_3MI vapor to a rather violent electric discharge at the exit of a supersonic expansion and it may be that the M−I bond does not stand up well to such abuse. In addition, the energies of the dissociation channels SiI + H and SiH + I are calculated to be very similar, so the opening of a second dissociation channel may influence the extent of the LIF spectrum.

HGeF. Both the barrier to dissociation and the bonding well are very small so, theoretically, only the 000 and the 010 vibrational levels are likely to exist for both isotopologues. This restriction suggests that either the LIF spectrum will not be observable or it will consist of no more that one or two bands which might fluoresce at energies low enough to preclude the formation of the GeF + H dissociation products. We have previously reported

unsuccessful attempts to observe the HGeF LIF spectrum using a H_3GeF precursor and by the reaction of germane with fluorine.[9]

HGeCl. In HGeCl, the barrier to dissociation is only ≈100 cm^{-1}, but the bonding well is ≈2500 cm^{-1}, sufficient to support several bending levels for both isotopologues. The experimental LIF spectra are in accord with the theoretical predictions, but tend to lose intensity 400 – 500 cm^{-1} below the dissociation barrier. Franck-Condon profiles of the absorption spectra, calculated in the harmonic approximation,[17] are in good agreement with the LIF data, indicating that the intensity tails off due to a diminution of vibrational overlap rather than the abrupt opening of a dissociation channel.

HGeBr. HGeBr has no significant barrier to dissociation and a bonding potential well of ≈ 3100 cm^{-1}, slightly larger than that of HGeCl. This prediction is reflected in the LIF spectra which extend 500 – 600 cm^{-1} further in HGeBr/DGeBr compared to HGeCl/DGeCl. Harmonic Franck-Condon calculations by Lin *et al*.[18,19] on both pairs of molecules show exactly this type of behavior, with the bending progression terminating after 2_0^3 in the hydrogen compounds and after 2_0^4 for the deuterated species, in accord with experiment. In HGeBr/DGeBr, it is again clear that the LIF spectra lose Franck-Condon intensity prior to the onset of dissociation.

HGeI. The potential energy surface of the $\tilde{A}\ ^1A''$ state has a deep bonding well of ≈ 3500 cm^{-1}, with a negligible barrier to dissociation. This property should in principle lead to an extensive absorption spectrum, but the experimental fact is that the LIF spectrum is not very lengthy (1800 cm^{-1}). As in the case of HSiI, this difference is probably due to the difficulty in producing HGeI in a discharge and the tailing off of the Franck-Condon profile well before the dissociation limit. In this case, we find the extra complication that the bending curve presents a swallow secondary minimum at θ_{HGeI}~60° (see Supplementary Material). The transition state reported in Table III connects the two minima along the bending coordinate and its energy is only ≈850 cm^{-1} above the main minimum of the $\tilde{A}\ ^1A''$ surface. In addition, the dissociation limits to GeI + H (24379 cm^{-1}) and GeH + I (25745 cm^{-1}) are energetically very similar, a feature found for all the HMI (M = Si, Ge, Sn) species (see Tables I - IV).

Despite these difficulties, the calculations clearly indicate that HGeI and DGeI should fluoresce and this prediction agrees with experiment.

HSnF. The $\tilde{A}\ ^1A''$ state of this molecule has both a barrier to dissociation and a bonding well smaller than 250 cm^{-1}, too limited to give rise to any bonded or quasi-bonded state. In Table IV, the predicted Max Energy for HSnF is negative, meaning that the zero-point energy is higher than the lowest vibrational level of the transition state. For DSnF, the zero-point level lies at slightly lower energies, but still very close to the transition state. These results lead to the firm prediction that HSnF and DSnF should not be observable by LIF spectroscopy. If the HSnF/DSnF molecules can be made in the gas phase, they will simply dissociate into hydrogen (deuterium) atoms and SnF molecules on excitation to the $\tilde{A}$ state, which should occur around 22 000 cm^{-1}.

HSnCl. Our calculations predict that only the 0-0 and possibly 2_0^1 bands of HSnCl and the 0-0, 2_0^1 and 2_0^2 bands of DSnCl should be observable in the bending progressions prior to the onset of molecular dissociation and an abrupt breaking off of the fluorescence. In recent experiments in the laboratory at Ideal Vacuum Products this is precisely what is observed,[13] with a single intense 0-0 band in the LIF spectrum of HSnCl, which exhibits a very short fluorescence lifetime, indicative of the near onset of dissociation. In DSnCl, the bending progression extends to 2_0^2, with decreasing fluorescence lifetimes up the vibrational manifold and loss of fluorescence at 458 cm^{-1} above the 0-0 level. The calculations give reliable values for the vibrational fundamentals in the ground and $\tilde{A}$ excited states (where known, see Table IV) and only slightly overestimate T_0 by 2.4% for both HSnCl and DSnCl. It is gratifying that the present theoretical results predict the extent of the LIF spectra and the effects of deuteration so well, lending confidence in the predictions for other as yet undetected HMX species.

HSnBr. The HSnBr/DSnBr species have deeper $\tilde{A}$ state bonding wells that the chloro--compounds and negligible dissociation energy barriers. This immediately leads to the prediction that the brominated species should have more extensive LIF spectra, ranging 1300 – 1500 cm^{-1} above the 0-0 band. It is likely that dissociation and loss of vibrational overlap intensity will be competitive factors in determining the observed extent of such spectra.

We note that a secondary minimum at a small bending angle was found, but it is at an energy larger than the SnBr + H dissociation and so it should not affect the LIF spectra.

HSnI. HSnI and DSnI are predicted to have significant bonding potential energy wells in the $\tilde{A}$ state without dissociation energy barriers, which would suggest that LIF spectra could be observed. However, in monoiodostannylene, we find similar but even more complexities in the potential energy surfaces than we found for HGeI. In addition to the large angle $\tilde{A}$ state minimum at 114°, there is a second small angle minimum at 46° which in this case is actually the global $\tilde{A}$ state minimum (378 cm^{-1} below the large angle minimum). The two competing dissociation channels are also energetically similar (SnI + H = 23 049 cm^{-1} and SnH + I = 24 957 cm^{-1}). Due to these difficulties, it has proven unrealistic to predict whether LIF spectra of HSnI or DSnI are likely to be observable

V. CONCLUSIONS

The main conclusion of this work is that whether or not the $\tilde{A}\,^1A''$ states of the HMX molecules fluoresce is determined primarily by the location of the excited state H (^{2}S) + MX ($X^2\Pi$) dissociation limit. The depth of the excited state potential energy bonding well and the existence of a barrier to dissociation (if any) can be rationalized as due to the extent of the mixing of the A″ components of the $^1\Delta$ and $^1\Pi$ states of the linear molecule configuration on bending.

A simple model based on perturbative second order theory proved to be sufficient to successfully explain the main features of the $\tilde{A}$ - $\tilde{X}$ electronic transition of the HMX/DMX (M=Si,Ge, X=F,Cl,Br) triatomics and reproduce their known spectroscopic constants. Such a model weakens for the iodine-containing species, for which the agreement is less satisfactory. This success supports a reliable prediction of the same spectroscopic properties for the corresponding tin-containing species.

Our calculations show that HGeF and DGeF dissociate very low down in the first excited singlet state and are unlikely to be detectable by LIF spectroscopy. The extent of the observable LIF spectra of the other HSiX and HGeX molecules is shown to be controlled as much by the slow diminution of the Franck-Condon factors as it is by the onset of HMX → H + MX dissociation channel. In the HSnX species, HSnF and DSnF are clearly dissociative and unlikely to fluoresce. In very good agreement with experiment, HSnCl is predicted to have a very limited LIF spectrum, which should be somewhat more extensive in DSnCl before the onset of dissociation. The calculations predict a deeper excited state bonding well for HSnBr/DSnBr and a more extensive LIF spectrum. Although the excited state potential energy well is even deeper for HSnI/DSnI, the *ab initio* results are complicated by a small angle global minimum and the opening of both H + SnI and HSn + I dissociation channels at similar energies. These difficulties make it impossible to make a definitive prediction as to whether the LIF spectra of HSnI and DSnI are likely to be observable, assuming that the iodo species can be made at all. Simple second order perturbation theory, which proved to be successful for the prediction of the spectroscopic behavior of most HMX species, is clearly not adequate for HMI species due to the complex shape of their first singlet excited state potential energy surface. For these latter, a more complex and computationally demanding variational approach will be mandatory. Finally, the yet unobserved triplet-singlet phosphorescence spectra of all the HMX molecules are calculated to occur in the 11000-16000 cm^{-1} range and are likely to be progressively stronger and perhaps observable with standard techniques for the germanium and tin species.

SUPPLEMENTARY MATERIAL:

See the Supplementary Material for (I) Frontier orbitals plots for all 12 HMX species, (II) Potential energy curves for the lowest states for all 12 HMX species and (III) Calculated spectroscopic parameters for HMX and DMX main isotopologues

AUTHOR'S CONTRIBUTIONS:

All authors contributed equally to this work.

ACKNOWLEDGEMENTS

The authors are grateful to Tony Smith of Ideal Vacuum Products, LLC for his continuing interest, encouragement, and financial support during the course of this research project. R.T. acknowledges financial support from the University of Bologna, and the from Italian MIUR (PRIN 2017, PHANTOMS project, Prot. 2017A4XRCA).

CONFLICTS OF INTEREST:

The authors have no conflicts to disclose.

DATA AVAILABILITY

The data that support the findings of this study are available within the article and in the supplementary material.

References:

1. W.W. Harper, J. Karolczak, D. J. Clouthier, and S. C. Ross, J. Chem. Phys. **103**, 883 (1995).

2. W.W. Harper, D. A. Hostutler, and D. J. Clouthier, J. Chem. Phys. **106**, 4367 (1997)

3. D. A. Hostutler, D. J. Clouthier, and R. H. Judge, J. Chem. Phys. **114**, 10728 (2001).

4. W. W. Harper and D. J. Clouthier, J. Chem. Phys. **106**, 9461 (1997)

5. D.A. Hostutler, N. Ndiege, D. J. Clouthier, and S. W. Pauls, J. Chem. Phys. **115**, 5485 (2001).

6. H. Harjanto, W. W. Harper, and D. J. Clouthier, J. Chem. Phys. **105**, 10189 (1996).

7. D. J. Clouthier, W. W. Harper, C. M. Klusek, and T. C. Smith, J. Chem. Phys. **109**, 7827 (1998).

8. B. S. Tackett and D. J. Clouthier, J. Chem. Phys. **118**, 2612 (2003).

9. W. W. Harper and D. J. Clouthier, J. Chem. Phys. **108**, 416 (1998).

10. B. S. Tackett, D. J. Clouthier, K. L. Pacheco, and G. A. Schick, J. Chem. Phys. **124**, 124320 (2006)

11. B. S. Tackett, Y. Li, D. J. Clouthier, K. L. Pacheco, G. A. Schick and R. H. Judge, J. Chem. Phys. **125**, 114301 (2006).

12. W. W. Harper, C. M. Klusek, and D. J. Clouthier, J. Chem. Phys. **109**, 9300 (1998).

13. G. Rothschopf, T. C. Smith and D. J. Clouthier, to be published.

14. T. C. Smith and D. J. Clouthier, J. Chem. Phys. **148**, 024302 (2018).

15. D. K. W. Mok, E. P. F. Lee, F.-T. Chau, and J. M. Dyke, J. Chem. Phys. **120**, 1292 (2004).

16. D. W. K. Mok, E. P. F. Lee, F-T. Chau, and J. M. Dyke, J. Chem. Theory Comput. **5**, 565 (2009).

17. D. K. W. Mok, F.-T. Chau, E. P. F. Lee, and J. M. Dyke, J. Comput. Chem, **31**, 476 (2010).

18 S.Lin, D. Xie, and H. Guo, J. Chem. Phys. **129**, 154313 (2008).

19. S.Lin, D. Xie, and H. Guo, J. Phys. Chem. A **113**,7314 (2009).

20. S. Lin and D. Xie, J Comput Chem, **32**, 1694 (2011).

21. M. Ehara, F- Oyagi, Y. Abe, R. Fukuda, and Nakatsuji, J. Chem. Phys. **135**, 044316 (2011).

22. A. Bundhun, P. Ramasami, and H. F. Schaefer III, J. Phys. Chem. A **113**, 8080 (2009)

23. A. Bundhun, P. Ramasami, P. P. Gaspar, and H. F. Schaefer, III, Inorg. Chem. **51**, 851 (2012).

24 a) H.-J. Werner, P. J. Knowles, G. Knizia, F. R. Manby and M. Schütz, WIREs Comput Mol Sci 2, 242 (2012); b) H.-J. Werner, P. J. Knowles, F. R. Manby, J. A. Black, K. Doll, A. Heßelmann, D.Kats, A. Köhn, T. Korona, D. A. Kreplin, Q. Ma, T. F. Miller, III, A. Mitrushchenkov, K. A. Peterson, I. Polyak, G. Rauhut, and M. Sibaev J. Chem. Phys. 152, 144107 (2020). c) MOLPRO, version 2010.1, a package of ab initio programs, H.-J. Werner, P. J. Knowles, G. Knizia, F. R. Manby, M. Schütz, and others, see https://www.molpro.net.

25. a) F. Neese, Wiley Interdiscip. Rev.: Comput. Mol. Sci. 2, 73 (2012); b) F. Neese, F. Wennmohs, U. Becker, and C. Riplinger, J. Chem. Phys. 152, 224108 (2020)

26. R. A. Kendall, T. H. Dunning, Jr., R. J. Harrison, J. Chem. Phys. **96**, 6796 (1992).

27. T. H. Dunning, K. A. Peterson, A. K. Wilson, J. Chem. Phys. **114**, 9244 (2001).

28. K. A. Peterson, D. Figgen, E. Goll, H. Stoll, M. Dolg, J. Chem. Phys. **119**, 11113 (2003).

29. F. Weigend and R. Ahlrichs, Phys. Chem. Chem. Phys., **7**, 3297 (2005).

30. H.-J. Werner and P. J. Knowles, J. Chem. Phys. **82**, 5053 (1985).

31. P. J. Knowles and H.-J. Werner, Chem. Phys. Lett. **115**, 259 (1985).

32. H.-J. Werner and P. J. Knowles, J. Chem. Phys. **89**, 5803 (1988).

33. P. J. Knowles and H.-J. Werner, Chem. Phys. Lett. **145**, 514 (1988).

34. E. R. Davidson and D. W. Silver, Chem. Phys. Lett. **53**, 403 (1977).

35. H.-J. Werner, M. Kallay and J. Gauss, J. Chem. Phys. **128**, 034305 (2008).

36. J. Senekowitsch, Ph.D. thesis, JohannWolfgang Goethe Universitat, Frankfurt am Main, Germany, 1988.

37. I. M. Mills. *Vibration-Rotation Structure in Asymmetric and Symmetric-Top Molecules*. In Molecular Spectroscopy: Modern Research, edited by K. N. Rao and C. W. Mathews, pages 115–140 (Academic Press, New York, 1972)

38. L. Laaksonen: *A graphics program for the analysis and display of molecular dynamics trajectories.* J. Mol. Graphics **10,** 33 (1992); D.L. Bergman, L. Laaksonen and A. Laaksonen: *Visualization of Solvation Structures in Liquid Mixtures*. J. Mol. Graphics & Modelling **15**, 301 (1997).

39. A. D. Becke, J. Chem. Phys. **98**, 5648 (1993).

40. C. Lee, W. Yang, and R. G. Parr, Phys. Rev. B **37**, 785 (1988).

41. H.-J. Werner, Mol. Phys. **89**, 645 (1996).

42. P. Celani and H.-J. Werner, J. Chem. Phys. **112**, 5546 (2000).

43. F. B. van Duijneveldt, J. G. C. M. van Duijneveldt-van de Rijdt, and J. H. van Lenthe, Chem. Rev. **94**, 1873 (1994).

44. Scott H. Kable, S. A. Reid and T. J. Sears, Int. Rev. Phys. Chem **28,** 435 (2009).

45. T.W. Schmidt, G. B. Bacskay and S. H. Kable, Chem. Phys. Lett. **292**, 80 (1998).

46. K. Sendt, T.W. Schmidt and G. B. Bacskay, Int. J. Quantum.Chem.**76**, 297 (2000)

47. G. B. Bacskay, J. Phys. Chem. **114,** 8625 (2010).

48. Luo, Y.-R. *Comprehensive Handbook of Chemical Bond Energies* (1st ed.). CRC Press, Boca Raton, 2007.

49. D. H. Mordaunt, H. Flöthmann, M. Stumpf, H.-M. Keller, C. Beck, R. Schinke and K. Yamashita, J. Chem. Phys. **107**, 6603 (1997).

50. O. Christiansen, T. A. Ruden, K. Ruuda and T. Helgaker, J. Chem. Phys. **116**, 8334 (2002).

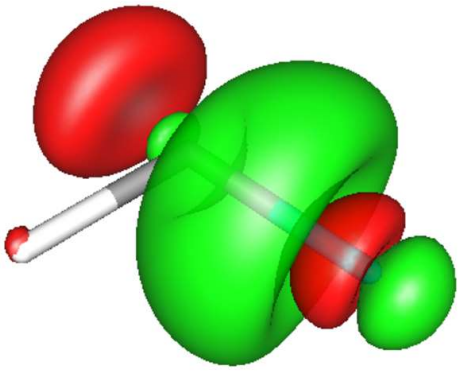

$a'_{\mathrm{LUMO+1}}$

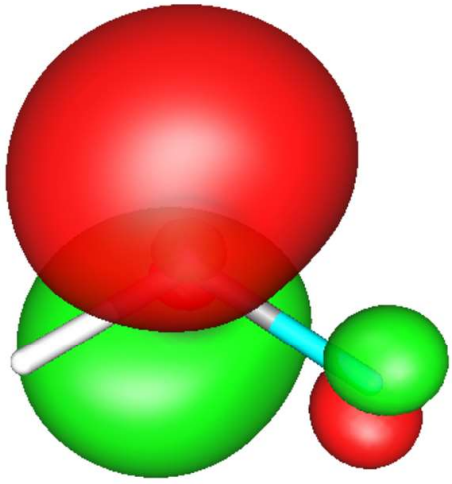

a''_{LUMO}

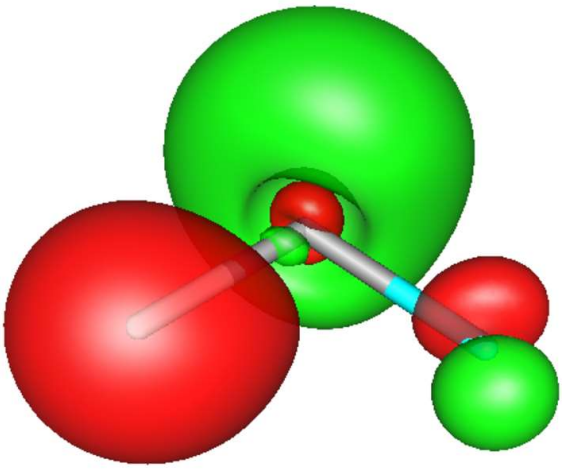

a'_{HOMO}

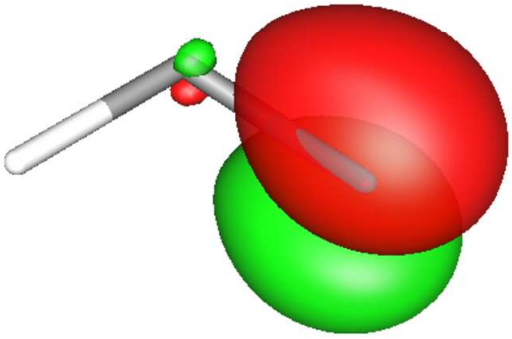

$a''_{\mathrm{HOMO-1}}$

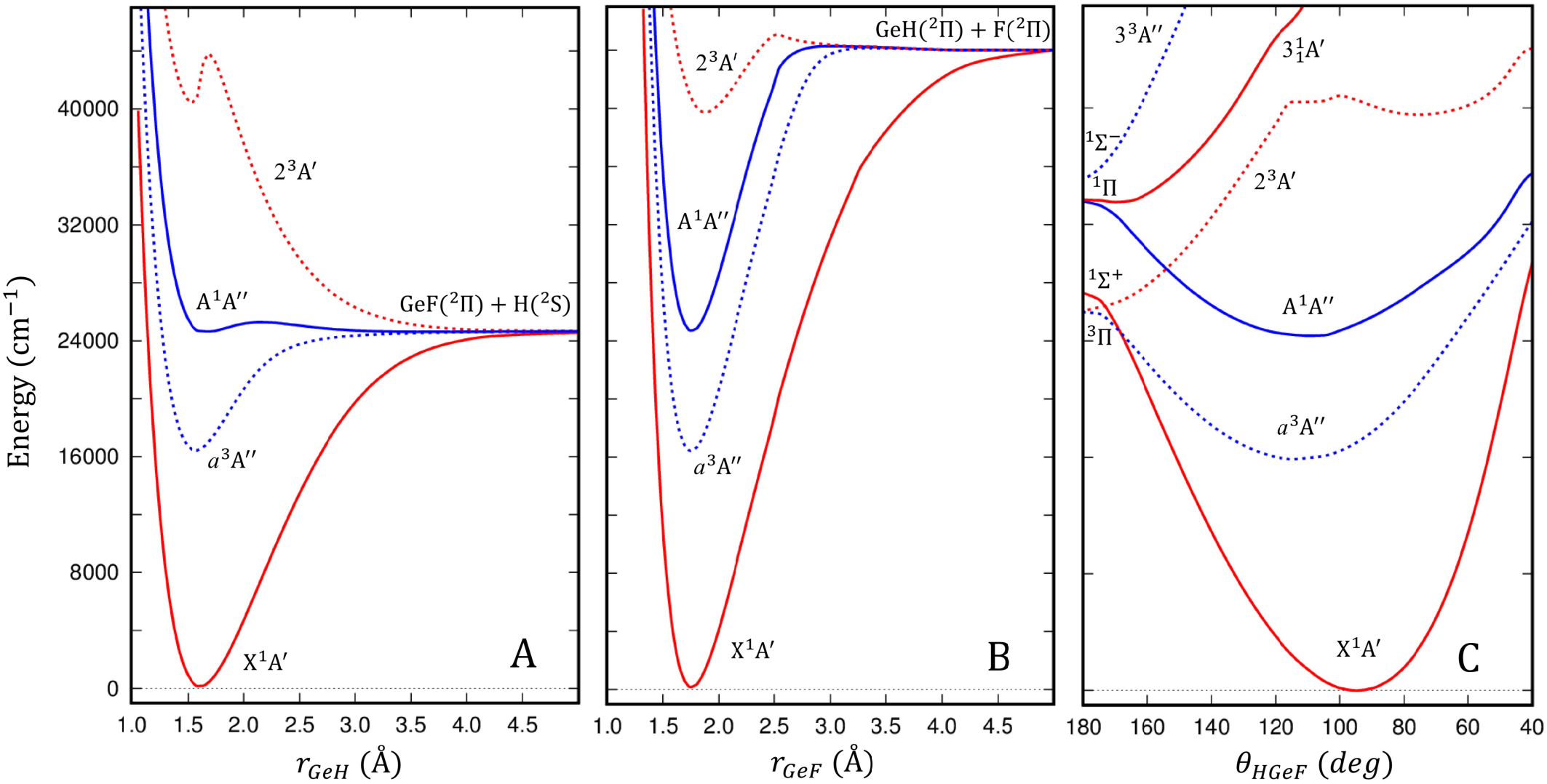
Energy (cm^{-1})
40000
32000
24000
16000
8000
0
2^3A′
A^{1}A″
GeF($^2\Pi$) + H(^{2}S)
a^3A″
X^{1}A′
A
1.0 1.5 2.0 2.5 3.0 3.5 4.0 4.5
r_{GeH} (Å)
GeH($^2\Pi$) + F($^2\Pi$)
2^3A′
A^{1}A″
a^3A″
X^{1}A′
B
1.0 1.5 2.0 2.5 3.0 3.5 4.0 4.5
r_{GeF} (Å)
3^3A″
3^1_1A′
$^1\Sigma^-$
$^1\Pi$
2^3A′
$^1\Sigma^+$
A^{1}A″
$^3\Pi$
a^3A″
X^{1}A′
C
180 160 140 120 100 80 60 40
θ_{HGeF} (deg)

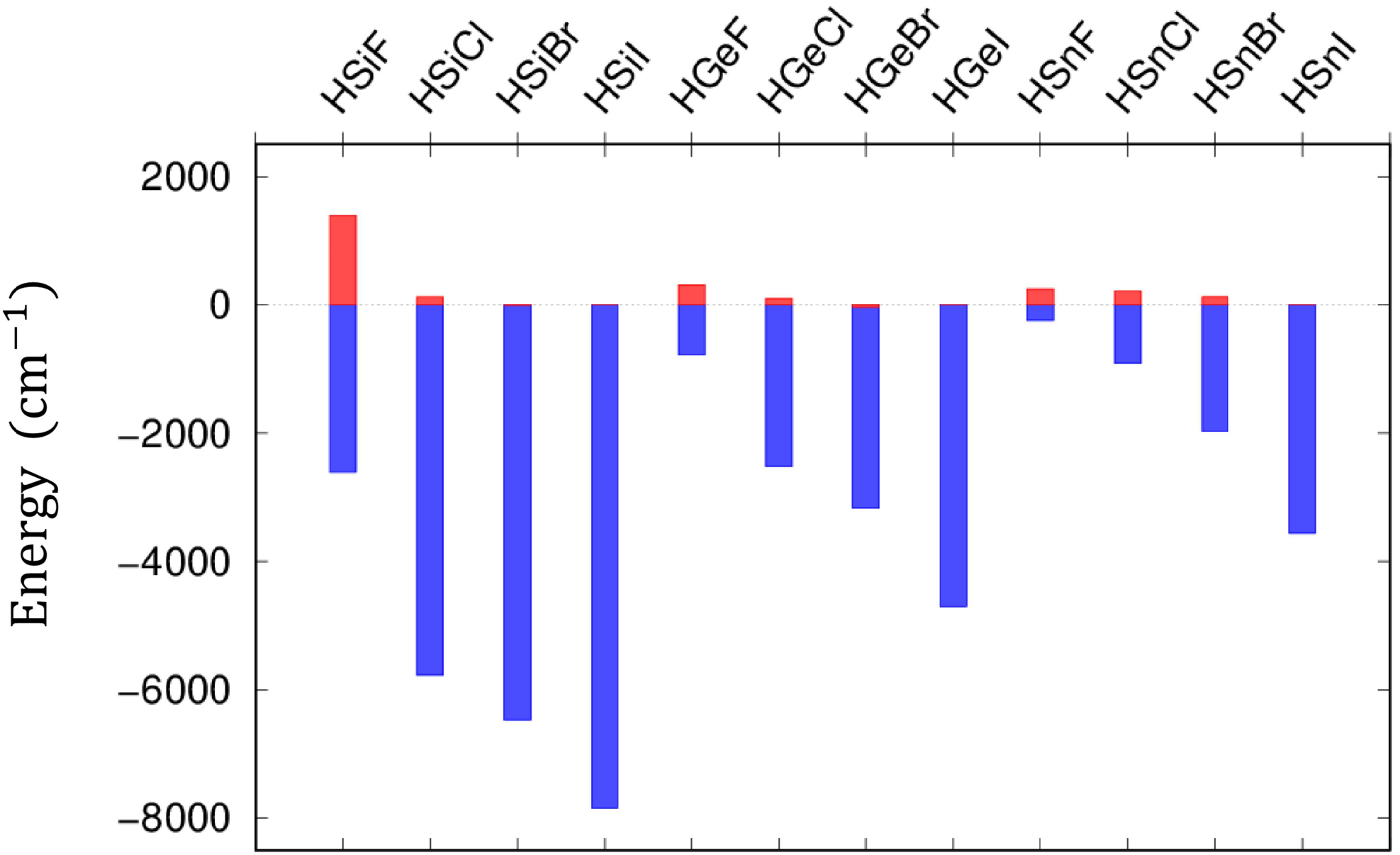
HSiF
HSiCl
HSiBr
HSiI
HGeF
HGeCl
HGeBr
HGeI
HSnF
HSnCl
HSnBr
HSnI
2000
0
−2000
−4000
−6000
−8000
Energy (cm^{-1})

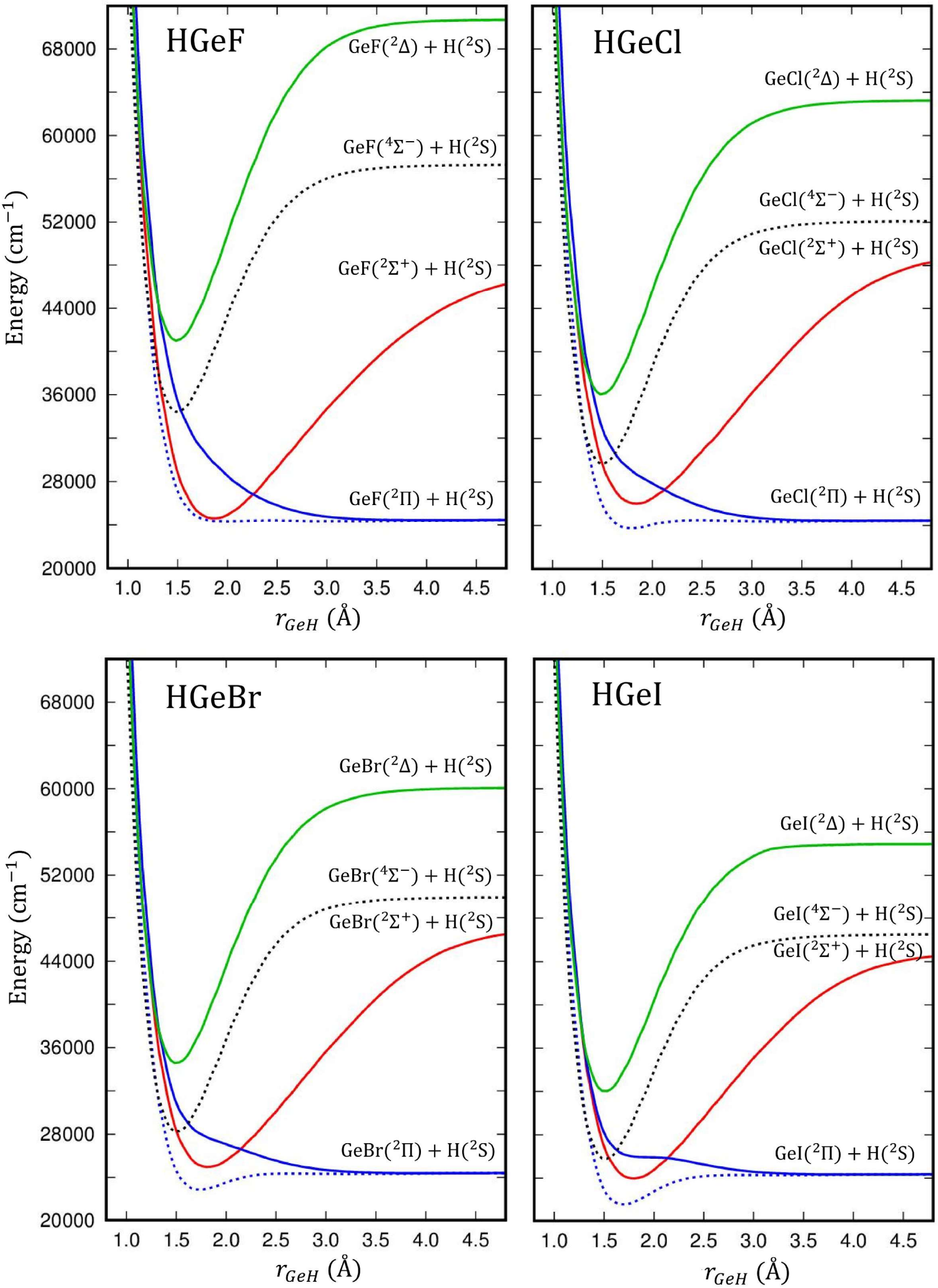
HGeF
GeF(²Δ) + H(²S)
GeF(⁴Σ⁻) + H(²S)
GeF(²Σ⁺) + H(²S)
GeF(²Π) + H(²S)
HGeCl
GeCl(²Δ) + H(²S)
GeCl(⁴Σ⁻) + H(²S)
GeCl(²Σ⁺) + H(²S)
GeCl(²Π) + H(²S)
HGeBr
GeBr(²Δ) + H(²S)
GeBr(⁴Σ⁻) + H(²S)
GeBr(²Σ⁺) + H(²S)
GeBr(²Π) + H(²S)
HGeI
GeI(²Δ) + H(²S)
GeI(⁴Σ⁻) + H(²S)
GeI(²Σ⁺) + H(²S)
GeI(²Π) + H(²S)
Energy (cm⁻¹)
20000
28000
36000
44000
52000
60000
68000
1.0
1.5
2.0
2.5
3.0
3.5
4.0
4.5
r_GeH (Å)

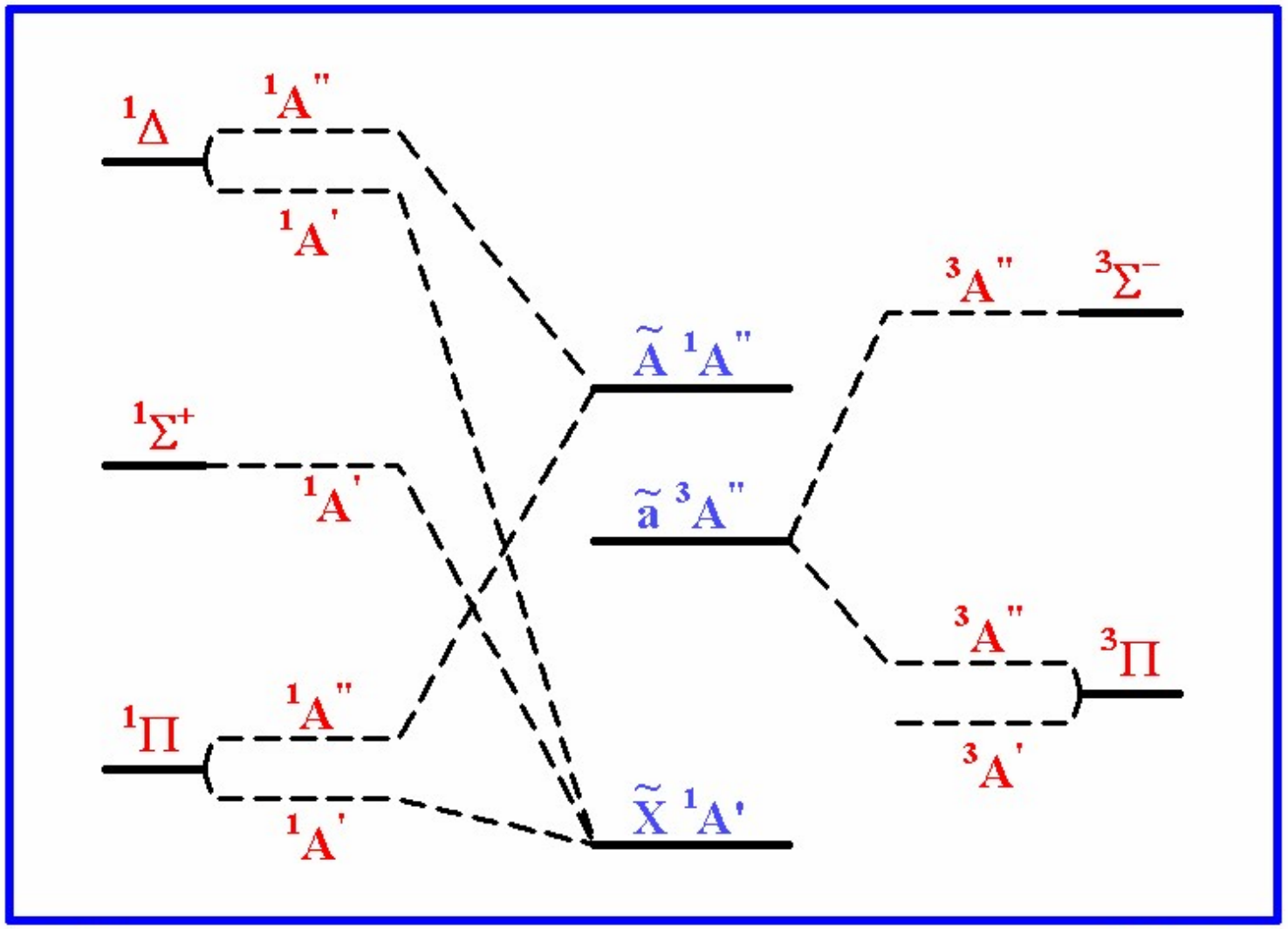
$^1\Delta$
$^1A''$
$^1A'$
$^1\Sigma^+$
$^1A'$
$^1\Pi$
$^1A''$
$^1A'$
$\tilde{A}\ ^1A''$
$\tilde{a}\ ^3A''$
$\tilde{X}\ ^1A'$
$^3A''$
$^3\Sigma^-$
$^3A''$
$^3\Pi$
$^3A'$
Linear Singlet States
Bent Molecule States
Linear Triplet States